

Metal Flow in Friction Stir Welding

Arthur C. Nunes, Jr.

Marshall Space Flight Center: EM30; Huntsville, AL 35812

Keywords: Friction Stir Welding, Shear Rate, Shear Surface, Rotating Plug Model, Wiping Mechanism

Abstract

The plastic deformation field in Friction Stir Welding (FSW) is compared to that in metal cutting. A shear surface around the FSW tool analogous to the metal cutting shear plane is identified and comprises the basis of the “rotating plug” flow field model and the “wiping” model of tool interaction with weld metal. Within the context of these models: The FSW shear rate is estimated to be comparable to metal cutting shear rates. The effect of tool geometry on the FSW shear surface is discussed and related to published torque measurements. Various FSW structural features are explained, including a difference in structure of bimetallic welds when alloys on the advancing and retreating sides of the weld seam are exchanged. The joining mechanism and critical parameters of the FSW process are made clear.

Introduction

The purpose of this paper is to report on a line of research in Friction Stir Welding (FSW) that is not as well known as it should be. This line of research reflects a philosophy that seeks to develop concepts that will assist the engineer in thinking creatively about the FSW process. Such concepts have to be simple and suggestive. A number of potentially useful concepts have come to light since we began to study the FSW process back around 1995. Some of these concepts are considered well established. Others are speculative. Some may generate controversy.

Tracer experiments make it clear that the flow around a FSW pin tool is not chaotic. Tracers flow along streamlines, albeit sometimes the streamlines can be very complex. K. Colligan [1] published a particularly illuminating tracer study of 0.38 mm steel shot in 6061 and 7075 aluminum in 1999. P. Heurtier *et al.* [2] have attempted recently to compute the approximate shape of some streamlines employing assumptions rather like the ones we make, although our model derives from plastic slip-line theory; theirs, from fluid mechanics.

The Shear Surface: The wiping Mechanism of Metal Transfer

The metal flowing around a FSW pin tool exhibits a sharp boundary between recrystallized and merely distorted areas [3] as shown in Figure 1. This sharp boundary suggests a velocity discontinuity or, rather, a very narrow zone of very high shear separating metal rotating with the pin from metal fixed in the weldment. At high strain rates metal processing maps exhibit regions of instability [4], where shearing is no longer homogeneous but concentrates in localized shear bands. When a local temperature rise occurs it makes local slip easier. The local shear rate then increases. If the local shear rate increment is able to produce a further local temperature rise sufficient to continue the easing of slip, the final result is that

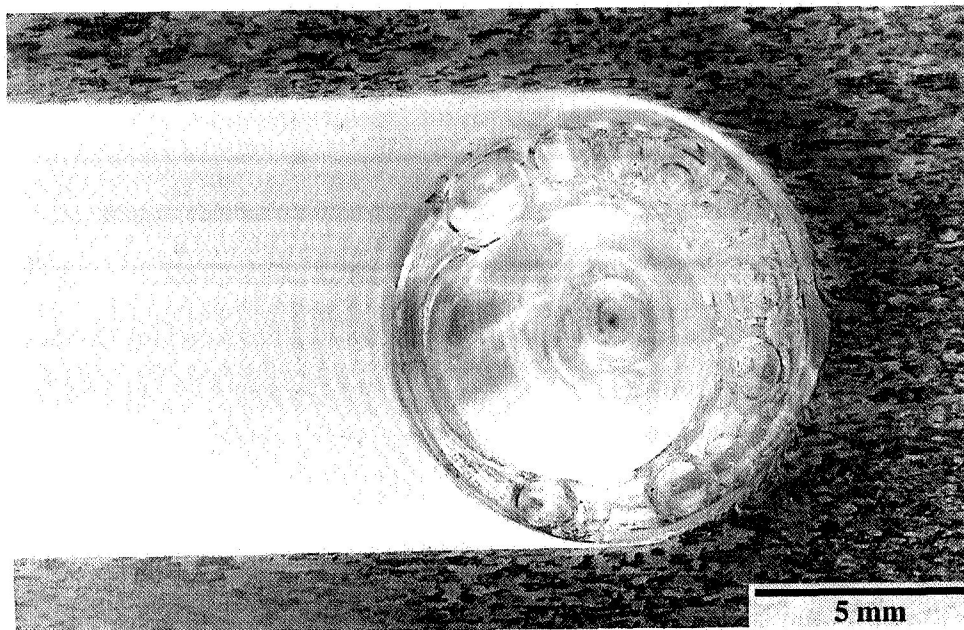


Figure 1: Mid-sectional macrostructure of FSW in 0.317 inch thick 2219-T87 aluminum alloy plate. The pin-tool has been removed and replaced with bubble-filled mounting medium. Rotation is in the counterclockwise direction. The spindle speed was 220 RPM and the travel speed 3.5 inches per minute.

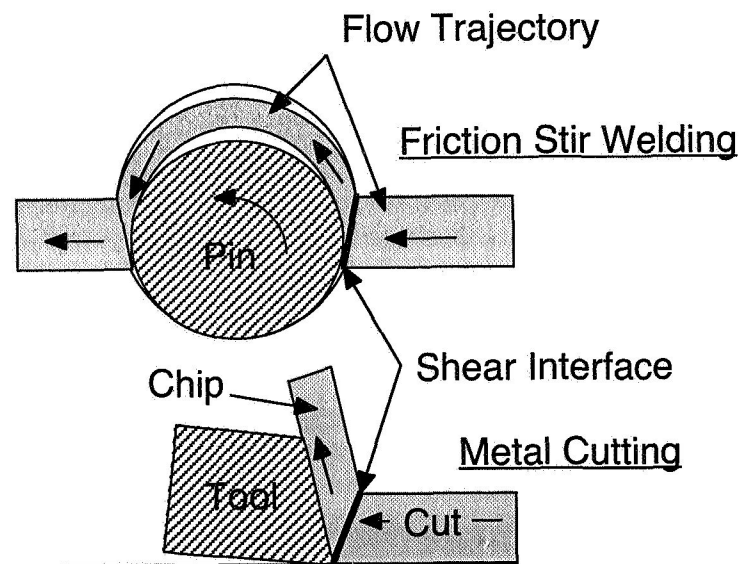


Figure 2: Comparison of FSW and metal cutting flow fields. The cylindrical shear surface around the FSW pin-tool and the metal cutting shear plane are corresponding zones of approximate velocity discontinuity or very high shear strain rate. The flow carried around the FSW pin-tool in the plug of metal rotating with the tool corresponds to the metal cutting chip. In both FSW and metal cutting the shear strain rate in the shear zones appears to be adequate to recrystallize the metal.

slip concentrates on a localized plane. The shear plane in metal cutting is an example of localized shear [5]. The FSW pin-tool appears to be surrounded by a shear surface that corresponds to the shear plane in metal cutting. FSW and metal cutting are compared in Figure 2.

The concept of a cylindrical shear surface separating metal rotating with pin and shoulder from the undisturbed part of the weldment can be seen as an application of plastic slip-line theory (Figure 3). This concept has turned out to be very helpful for understanding a number of features of friction stir welding that seem complicated at first glance.

The shear surface moves with the tool. As the tool moves into and engulfs new metal, the metal newly attached to the tool is rotated with the tool. The newly attached metal is abandoned behind the tool. This mechanism by which metal encountered at the front of the tool is moved behind the tool has been named the “wiping mechanism” of metal transfer. The metal is wiped onto the metal rotating with the tool and is wiped off onto the weldment at the back of the tool. The flow field around the tool bulges slightly on the retreating side of the tool as shown in Figure 3, because it is on the retreating side that the metal is carried back around the tool.

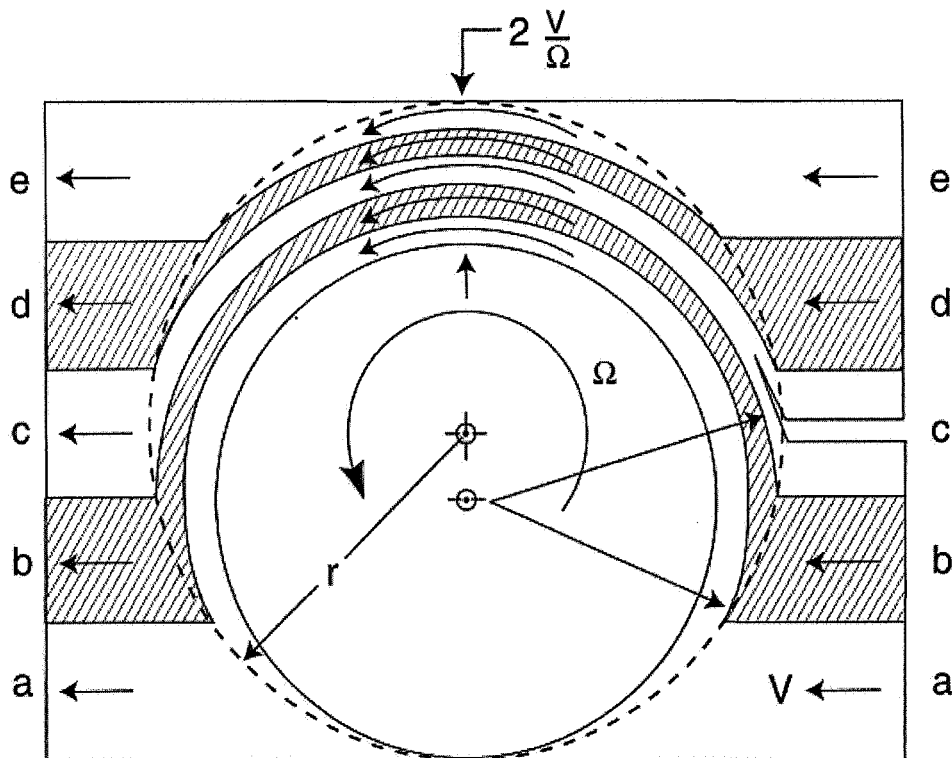


Figure 3: Two-dimensional “wiping” flow streamlines for a FSW flow field. The width of the pattern has been greatly exaggerated to reveal the structure more clearly. In the typical FSW case the flow around the tool takes place within a thin sliver of rotating metal just beneath the shear surface.

For a two-dimensional flow with shear zone radius R and with translational velocity V the volume flow rate captured by a unit length of shear zone is approximately $2RV$ (ignoring axial flow). The volume flow rate back past the retreating edge of the pin is approximately $R\Omega\delta$, where δ is the height of the

bulge on the retreating surface and Ω is the angular velocity of the pin. Equating the two volume flow rates yields a bulge height of δ .

$$\delta \approx \frac{2V}{\Omega} \quad (1)$$

If V is 3.5 inches per minute and Ω is $\left(2\pi \frac{\text{rad}}{\text{rev}}\right)(220\text{RPM})$ as for Figure 1, then δ is around 0.005 inches (124 microns). The value of δ measured from the photograph in Figure 1 is on the order of 0.008 inches (200 microns). The measured δ is somewhat larger than the theoretical computation above, but the above computation neglects axial flow. If a mean axial flow V_A down the tool is included in the continuity equation, then agreement with a measured δ can be obtained by the incorporation of a gradient in the axial velocity, such that

$$\frac{\partial V_A}{\partial z} \sim \frac{2V}{\pi\delta} \left(\frac{1 - \frac{1}{2} \frac{\delta\Omega}{V}}{1 - \frac{1}{4} \frac{\delta}{R}} \right) \quad (2)$$

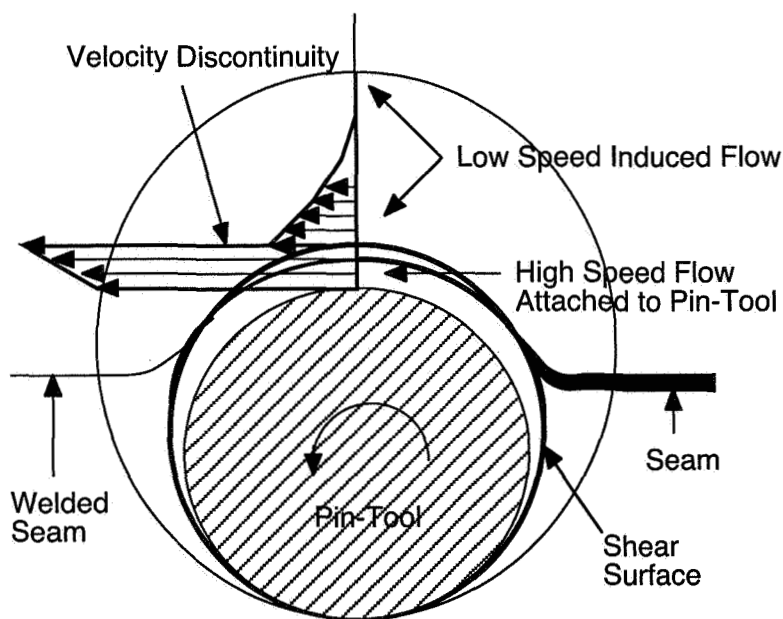


Figure 4: Induced flow in the vicinity of the pin-tool causes preliminary distortion of the seam before it enters the shear zone and is welded.

The measured value of δ from Figure 1 agrees with theory if a decelerating axial velocity gradient of around -163 inches per minute per inch holds within the rotating plug. The decreasing axial flow accumulates extra metal in the plug of metal rotating with the tool. The extra metal influx broadens the bulge of rotating metal on the retreating side.

This model is approximate, of course. Observations show a zone of relatively slow shearing rate surrounding the shear interface (Figures 4 and 5). We take this zone to be a presumably viscous or creeping flow induced by shear forces at the shear interface and promoted by the raised temperatures due to the heat generated in the shear zone. One sees similar “induced” deformation surrounding the shear zone in metal cutting, although it has generally not been so labeled. It is possible for a tracer in the path of the FSW tool to be swept around the tool in the induced flow without passing through the shear zone itself.

An attempt to compute an extended distribution of angular velocity also leads to the concept of a shear interface. The torque needed to rotate a unit length of a cylinder of metal of radius r with shear flow stress τ is $2\pi r^2\tau$. Equilibrium of a thin ring of weld metal rotating around the FSW pin requires that moments on inner and outer surfaces balance, i.e. that $\frac{\partial}{\partial r}(2\pi r^2\tau) = 0$, if the ring is not to accelerate and the angular velocity is to remain stable. This implies that for slip to occur over an extended region $\tau \propto \frac{1}{r^2}$.

Compared to temperature effects it is well known that the shear stress in metals is not very sensitive to shear rate. For example Nadai [6] exhibits plots of true yield and ultimate tensile stress of mild steel at room temperature over a range of strain rates $\dot{\epsilon}$ of 9 orders of magnitude; the ultimate tensile strength UTS, more like a flow stress than the yield strength due to the greater amount of deformation associated with it, increases by about 50% over the entire range. At the high-end strain rate, 10^3 per second, the slope rises to $\frac{dUTS}{d\log_{10}\dot{\epsilon}} \approx 9,000$ psi. A theoretical rationale for logarithmic dependence can be made for a range of strain rates limited to a single dislocation mechanism[7]. Let it be noted that this is quite different from viscous behavior where the stress depends linearly on the strain rate.

The temperature has to drop with radial distance from the tool for heat to flow away from the tool, where it is generated, into the weld metal. This drop in temperature causes hardening of the weld metal and an increase in τ with radius r . The equilibrium condition for extended slip, $\tau \propto \frac{1}{r^2}$, is not met unless somehow the angular velocity can drop fast enough to reduce τ proportionally to $\frac{1}{r^2}$. Considering the small effect of strain rate on stress in metals, a precipitous drop in angular velocity not much different from a discontinuity would be required. It was this consideration that originally suggested to the author to consider a shear discontinuity of flow around the FSW pin-tool.

How the FSW Process Works

The FSW process is a solid-state process like the hammer welding process of blacksmiths. The blacksmith heats the metal to make it soft, then hammers it into intimate contact. By the nature of the metallic bond, clean metal surfaces join when put into contact.

In FSW the seam is stretched way out as it crosses the shear surface as shown schematically in Figure 5. As a length of seam $V \cos\theta\Delta t$ crosses the shear surface the outermost part is carried laterally by distance $R\Omega\Delta t$. If the original seam is 100% covered with contaminants that prevent bonding, the level of residual contamination on the expanded surface is

$$\frac{V \cos \theta \Delta t}{\sqrt{(R\Omega\Delta t)^2 + (V \cos \theta \Delta t)^2}} \approx \frac{V \cos \theta}{R\Omega} \quad (3)$$

For typical FSW parameters this is just a few percent or less; a clean surface is generated and only needs to be forced together with sufficient pressure so that the contact area encompasses the whole surface.

According to slip-line plasticity theory a contact pressure of roughly 3 times the linear flow stress at the joint surface or 6 times the local shear stress is needed to push down a surface asperity due to the constraint of the surrounding metal. This is the minimal pressure required to put metal surfaces into full contact. The deformation takes place at the shear surface where the heat generated by intense plastic deformation produces temperatures approaching, but not reaching melting. The flow stress of hot metal can become very small. If the flow stress in shear is on the order of 1000 psi, then the contact pressure p required to weld clean metal is on the order of 6000 psi.

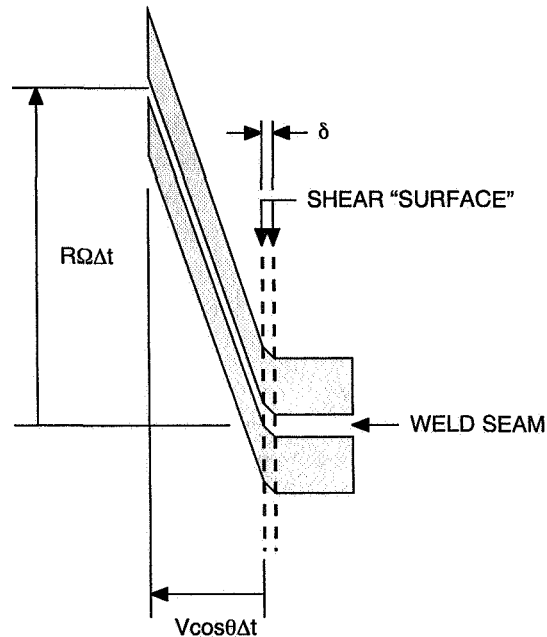


Figure 5: The weld seam is expanded by a factor of approximately $\frac{R\Omega}{V \cos \theta}$ upon crossing the shear surface. This exposes the clean metal needed for making a sound weld.

The axial plunge force can produce the needed contact pressure. The pressure is then symmetrically distributed around the pin-tool and does not contribute to the tool drag, which can be very low. Forcing the tool forward against the incoming metal can also produce the contact pressure, but this increases the drag pressure p_D on the pin. It is needed to make up insufficiency in the symmetrical plunge force pressure p , i.e. $p_D = \frac{\tau}{\mu} - p$. This simple picture is, however, a great oversimplification. It does seem to be

the case that loss of plunge force pressure increases drag, but other factors complicate measured tool drag. A better understanding of flow configurations in contact with the tool shoulder seems to be a key desideratum.

The Shear Rate: Relation to Metal Cutting

The shear rates in metal cutting are reputed to be in the range from 10^3 to 10^5 per second and sometimes as high as 10^7 [8]. Comparable rates would be anticipated in the friction stir welding process.

Given a weld speed V , at an angle θ away from the translation direction metal approaches the shear surface at a speed $V \cos \theta$. In a unit time increment Δt a height of metal $V \cos \theta \Delta t$ enters the rotating field and is displaced perpendicularly to the inflow direction by $R\Omega \Delta t$, where R is the radius of the shear surface and Ω , the angular velocity of the metal inside the shear surface. Ω is the same as the angular velocity of the tool if there is no slipping between the shear surface and the tool. The shear increment $\Delta \gamma$ is then $\frac{R\Omega}{V \cos \theta}$. The shear takes place during the crossing of the shear zone. If the shear

zone width is δ , then the time increment Δt to cross the zone is $\frac{\delta}{V \cos \theta}$. Hence the rate of shear is

$$\frac{d\gamma}{dt} = \frac{\Delta \gamma}{\Delta t} = \frac{\left(\frac{R\Omega}{V \cos \theta} \right)}{\left(\frac{\delta}{V \cos \theta} \right)} = \frac{R\Omega}{\delta} \quad (4)$$

If R is 0.25 inches, Ω is $\left(2\pi \frac{\text{rad}}{\text{rev}} \right) (200\text{RPM})$, and δ is 0.005 inches, then the shear rate is on the order of 10^3 per second.

Presumably it is this high strain rate that gives rise to the finely recrystallized grain nanostructure in the wake of the weld. Dislocations may be visualized emerging from sources located in grain boundary or sub-grain boundary dislocation concentrations. The emergent dislocations move along those crystal planes most closely parallel to the shear surface so as to generate the velocity discontinuity at the shear surface. Dislocations of opposite sign run in opposite directions. Occasionally a pair of opposing dislocations may encounter one another closely enough to lock together. Locked dislocations in the center of parent grains create a basis for a new refined set of grains while most dislocations simply annihilate one another with the emission of elastic waves observed as heat. Development of a quantitative dislocation model of deformation at the shear surface could, it is proposed, lead to understanding of the FSW recrystallization process.

If the high strain rate attributed to the FSW process results in a very small grain structure, then one would expect to find a similar very small grain structure in metal-cutting chips. This is apparently the case. Researchers at Purdue University have proposed using metal-cutting chips as a source of nanostructured metals [9]. It should be noted, however, that actual metal-cutting chips, unlike the FSW analogue of the metal-cutting chip, have a free surface. Hence some structural differences should be anticipated.

Shear Surface Shape

If a control volume is drawn separating the friction stir tool and any weld metal fixed to it the torque M required to rotate the tool is

$$M = \int_{\text{Control Volume}} 2\pi r^2 \tau \sqrt{dr^2 + dz^2} \quad (5)$$

In equation 5, r and z are radial and axial coordinates of the surface ($r = r(z)$) and τ is the shear flow stress on the shear surface. If the tool can rotate at a given power, all modes of rotation requiring more power are circumvented. Hence the rotation is assumed to take place at the configuration $r(z)$ for which torque is a minimum.

$$\delta \int_{\text{Control Volume}} 2\pi r^2 \tau \sqrt{1 + r'^2} dz = 0 \quad (6)$$

In equation 6, $r' \equiv \frac{dr}{dz}$.

If the temperature field is approximately constant over the shear surface and if the flow stress is negligibly affected by strain rate differences, the flow stress on the shear surface does not vary, then, applying calculus of variations, a differential equation for the shape of the shear surface is obtained.

$$r\ddot{r} - 2\dot{r}^2 - 2 = 0 \quad (7)$$

The solution is an elliptic integral [10] of the first kind $F(\varphi \setminus \alpha)$.

$$z = aF(\varphi \setminus \alpha) \quad (8)$$

In equation 8, $\varphi = \cos^{-1}\left(\frac{a}{r}\right)$, $\alpha = 45^\circ$, a is a constant that can be used to fit boundary conditions, and z is taken equal to 0 when $r = a$. Below $z = 0$ the solution on the sides of the pin becomes a straight-sided cylinder, $dr = 0$, with minimal r . On the bottom of the pin the shear surface is flat and circular in this model. A sample surface contour is shown in Figure 6. Such contours are commonly seen in axial and lateral sections of emergency-stopped weld sites.

In this simplified model below the shear disc at the bottom of the pin the seam is passed over unwelded. In reality the metal beneath the pin is appreciably deformed, but not necessarily enough to produce a high quality bond. If the frictional shear stress on the anvil surface is less than the shear flow stress within the weld metal, however, at a critical distance between anvil and pin bottom the shear surface drops down to the to the anvil and the defective region under the pin disappears [11].

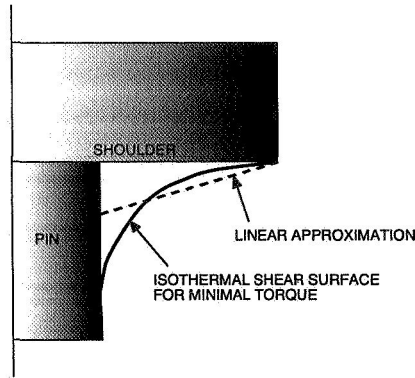


Figure 6: The computed shear surface shape (solid line) yielding minimal torque/power for isothermal/constant flow stress FSW tool environment. A simplified linear approximation (dashed line) is also shown.

Flow Stress on the Shear Surface

If the shear flow stress τ and the shape of the shear surface are known, moment M and power $M\Omega$ can be computed for a given weld. For empirical power measurements [12] made by Reynolds and Tang and using a linear approximation to the shear surface shape it is possible to compute shear flow stress values τ that fit the empirical data best. The results of these computations are shown in Table I.

Table I. Effect of Friction Stir Welding Tool Configuration on Power Requirement. Percent error in the computed value in parenthesis next to compared values.

Tool Configuration	Power Requirement (watts)								
	240 RPM/1.3 mm/sec $\tau = 2.01$ ksi*			240 RPM/2.4 mm/sec $\tau = 2.18$ ksi*			390 RPM/3.3 mm/sec $\tau = 1.75$ ksi*		
	Measured	Computed		Measured	Computed		Measured	Computed	
1	2060	1870	(-9%)	2230	2030	(-9%)	2790	2660	(-5%)
2	1950	1670	(-14%)	2100	1840	(-12%)	2790	2400	(-14%)
3	2270	2050	(-10%)	2390	2230	(-7%)	2860	2910	(+2%)
4	1110	1180	(+6%)	1260	1280	(+2%)	2290	1670	(-27%)
5	2310	2910	(+26%)	2560	3160	(+23%)	3040	4130	(+36%)

* Chosen for optimal data fit.

The flow stress is of a reasonable order of magnitude, although good comparison data on flow stresses at temperatures so near melting is lacking. The optimal-fit flow stress goes up a bit with weld speed and down significantly with tool RPM, apparently affected by temperature as anticipated.

The level of agreement between empirical and computed power is judged not too bad considering the rough assumptions and the simplicity of the computation. Distinctly greater error is associated with the

widest shoulder (Configuration 5); the power is overestimated in all three cases. This suggests slippage at the edge of the widest shoulder at stresses less than the metal flow stress.

Bimetallic Welds

Given a pure rotation of angular velocity Ω plus a radially outward velocity u inside a shear surface of initial radius R_o and exiting radius R all swept along at weld speed V , the lateral displacement Δy of an element of weld metal by the rotational field is approximately (treating r as R_o):

$$\frac{\Delta y}{R_o} = \frac{R_o \Omega}{2V} \left[1 - \left(\frac{R}{R_o} \right)^2 \right] + \frac{1}{R_o} \frac{u}{V} \int r d\theta \sim \frac{R_o \Omega}{2V} \left[1 - \left(\frac{R}{R_o} \right)^2 \right] + \frac{u}{V} \Delta \theta \quad (9)$$

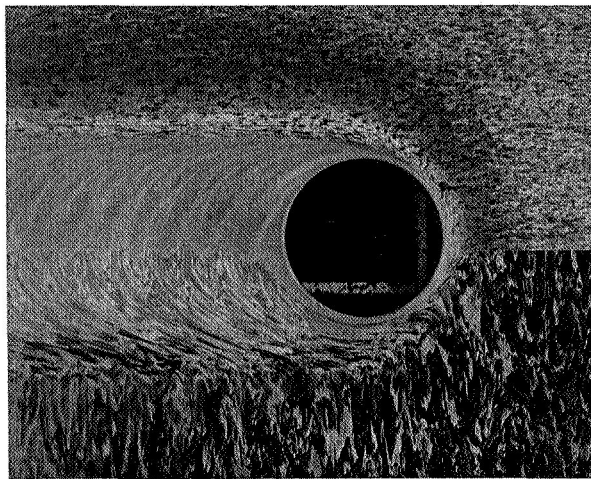


Figure 7: Plan midsection of bimetallic friction stir weld. On the upper, advancing side is 2219 aluminum alloy; on the lower, retreating side is 2195 alloy. The pin site or central hole is 12.7 mm (0.5 inch) in diameter (Courtesy of G. Bjorkman of Lockheed Martin.)

The displacement is positive in the direction of the retreating side of the tool. Radial inflow near the shoulder (negative u) tends to shift tracers toward the advancing side; the reverse is true for radial outflow at the pin bottom. Changes in shear surface radius can offset this. There is a lot of evidence for shear surface oscillations.

Figure 7 shows a plane midsection of a binary weld courtesy of G. Bjorkman of Lockheed Martin. On the advancing side of the weld seam the weld metal is 2219 aluminum alloy; on the retreating side, 2195 alloy. The seam trace between metals in the wake of the weld shows some oscillations but is not much displaced from the initial seam. The 2219 alloy on the advancing side is recrystallized in flow close to the tool. The 2195 alloy on the retreating side is highly distorted but not recrystallized in the tool wake. The 2195 backflow around the tool extends out a distance of roughly half a tool radius beyond the tool.

Balancing volumetric flow rates into and back around the tool implies a mean backflow velocity of the order of three times the weld speed, nowhere near the rotational surface speed of the tool. It would appear that the shear surface remains inside the (softer?) 2219 alloy while the (harder?) 2195 alloy is swept around the shear surface in a slower peripheral flow lacking a shear rate sufficient for recrystallization! Where the 2195 alloy is on the advancing side, without an initial buildup of a sublayer of 2219 alloy, the 2195 alloy appears to support a recrystallizing shear surface and both the 2195 and the 2219 sides of the weld exhibit recrystallization.

Conclusion

The concept of a shearing surface analogous to the metal cutting shear plane surrounding the FSW pin-tool and separating weld metal attached to and rotating with the tool from the rest of the weld metal appears reasonable from the point of view of the continuum mechanics of metals and from observations of FSW macro/microstructures. Brief demonstrations in this paper illustrate the use of this concept in analysis of the dependence of torque on FSW tool geometry and a peculiar feature observed in bimetallic welds. Other applications have been published by the author [11]. Tracer studies by J.A. Schneider of Mississippi State University [13] and FSW drag and plunge force studies by J.C. McClure of the University of Texas at El Paso [14] applying the shear surface concept are underway. Many researchers have assisted in the development of the shearing surface concept in FSW, but the most current work is embodied in that of the latter two researchers.

References

1. K. Colligan, "Material Flow Behavior during Friction Stir Welding of Aluminum," *Welding Journal* 78 (7) (1999) Research Supplement 229-s to 237-s.
2. P. Heurtier et al., "Mechanical and thermal modeling of Friction Stir Welding," *Journal of Materials Processing Technology* 176 (2006) 348-357.
3. R.W. Fonda, J.F. Bingert, and K.J. Colligan, "Development of Grain Structure during Friction Stir Welding," *Scripta Materialia* 51 (2004) 243-248.
4. Y.V.R.K. Prasad and S. Sasidhara, eds., *Hot Working Guide: A Compendium of Processing Maps* (Materials Park, OH: ASM International, 1997) 6-10 and passim.
5. P.L.B. Oxley, *The Mechanics of Machining: An Analytical Approach to Assessing Machinability* (New York, NY: Halsted Press, a division of John Wiley & Sons. 1989) 23-63.
6. A. Nadai, *Theory of Flow and Fracture of Solids* vol.1, Second Edition, (New York, NY: McGraw-Hill Book Company, Inc. 1950) 315.
7. A.C. Nunes, Jr. et al., "Effect of Strain Hardening on the Low-Temperature Thermally Activated Deformation Mechanisms in Polycrystalline Aluminum," *Transactions of the American Society for Metals* 58 (1) (1965) 38-45.

8. P.H. Cohen, "Forces, Power, and Stresses in Machining," *Metals Handbook, Vol. 16* (Metals Park, OH: ASM International, 1989) 13-18.
9. T.L. Brown, et al., "Low-cost manufacturing process for nano-structured metals and alloys," *Journal of Materials Research* 17 (10) (2002), 2484-2488.
10. L.M. Milne-Thomson, "Jacobian Elliptic functions and Theta Functions," *Handbook of Mathematical Functions With Formulas, Graphs, and Mathematical Tables, Third Printing with Corrections*, ed. M. Abramowitz and I.A. Stegun (Washington, DC: National Bureau of Standards, 1965), 567-626.
11. A.C. Nunes, Jr., "Wiping Metal Transfer in Friction Stir Welding," *Aluminum 2001: Proceedings of the 2001 TMS Annual Meeting* (New Orleans, LA, February 11-15) *Automotive Alloys and Joining Aluminum Symposia*, ed. G. Kaufmann, et al. (Warrendale, PA: The Minerals, Metals & Materials Society, 2001) 235-248.
12. A.P. Reynolds and Wei Tang, "Alloy, Tool Geometry, and Process Parameter Effects on Friction Stir Weld Energies and Resultant FSW Joint Properties," *Friction Stir Welding and Processing*, ed. K.V. Jata et al. (Warrendale, PA: The Minerals, Metals & Materials Society, 2001) 15-23.
13. J.A. Schneider and A.C. Nunes, Jr., "Influence of processing parameters on the flow path in friction stir welding." Submitted to *Science and Technology of Welding and Joining*.
14. J.C. McClure, "A Study of Forces during Friction Stir Welding" (Report NASA Summer Faculty Research Opportunities, Marshall space Flight Center, 2005)